Environ Earth Sci (2015) 74:6887–6899
DOI 10.1007/s12665-015-4691-1

ORIGINAL ARTICLE

Shear strength of shale weathered expansive soils along swell-shrink paths: analysis based on microscopic properties

Botao Lin[1] · **Amy B. Cerato**[2]

Received: 17 October 2014 / Accepted: 19 June 2015 / Published online: 7 July 2015

Abstract This study attempts to interpret the macro-scale mechanical behavior of two natural expansive soils based on their microscopic properties. To accomplish this, an extensive investigation on the microscopic properties, including physicochemical properties, especially point of zero charge and microstructural characteristics observed from environmental scanning electron microscopy, was carried out in order to understand the sample fabric and the interparticle forces affecting it. Furthermore, triaxial tests were conducted on the saturated and unsaturated specimens to evaluate their strength behavior with respect to the governing microscopic forces and microstructure. The effects of mean stress, suction, capillary history and strain level on the shear strength were thoroughly examined. It was found that the initial sample structure has a profound impact on the development of effective stress paths of the saturated specimens. For the sample with a flocculated structure, capillary history causes substantial structural evolutions along different capillary paths, and consequently results in significant changes in the peak shear strength. For the laminar sample, the impact of capillary history is negligible on its peak strength. On the other hand, the large-strain shear strength is insensitive to capillary history, regardless of soil type because the specimens are fully destructed with respect to their fabric, experiencing a loss of electrical attraction and equilibrium of diffuse double layer repulsion.

Keywords Shale · Expansive soils · PZC · Microstructure · Wetting/drying · Swell/shrink · Shear strength

✉ Amy B. Cerato
acerato@ou.edu

Botao Lin
linbotao@vip.163.com

[1] State Key Laboratory of Petroleum Resources and Prospecting, China University of Petroleum, Beijing 102249, China

[2] School of Civil Engineering and Environmental Science, University of Oklahoma, Norman, OK 73019, USA

Introduction

Expansive soil is defined as any soil or rock material that has a potential for swelling or shrinking under changing moisture conditions (from Nelson and Miller 1992). A standard threshold of swell or shrink potential above which a soil is considered expansive does not exist in part because the tests used to evaluate swell or shrink potential create variable sample conditions. In the literature, swell potential of expansive soil samples has been evaluated using various moisture content, density or surcharge loading, resulting in a vast range of values from less than 0.5 % to more than 30 % (e.g., Nelson and Miller 1992; Al-Rawas 1999; Punthutaecha et al. 2006; Zhan and Ng 2006; Nowamooz and Masrouri 2008; Ito and Azam 2010). Therefore, the shrink and swell potential of expansive soil simply refers to its relative capacity for expansion or contraction.

Natural expansive soil, as a weathered product of shale or mudstone, volumetrically expands or shrinks upon adsorption or desorption of water. Such a behavior causes damage to foundations of structures, bridges and roads, or induces potential landslides along transportation corridors. Expansive soil becomes a preferable material, however, when used as impervious liners for canals or irrigation ducts, engineered clay barriers for nuclear waste repositories or landfills, owing to its extremely low hydraulic

permeability. Besides its role in the civil engineering arena, expansive soil also draws research interests in the field of petroleum engineering, since physicochemical and mechanical features of clay minerals are crucial in studying the capacity of drilling fluid and the stability of exposed shale formations at the borehole wall (Fjar et al. 2008).

Difficulty is encountered in physically predicting the macroscopic mechanical responses of expansive soil because of the high composition of clay platelets/aggregates. Surface physicochemical forces, rather than mechanical contact forces, of these clay platelets/aggregates govern the macro scale behavior due to the micron size (<2 μm) of clay particles and the diffuse double layer (DDL). As such, it is desirable to understand the microscopic mechanisms through which these physicochemical forces determine the macroscopic behavior of an expansive soil sample given a specific microstructure. In the literature (e.g., Escario and Saez 1986; Delage et al. 1998; Wiebe et al. 1998; Tang et al. 2002; Blatz et al. 2002; Tripathy et al. 2002; Tripathy and Subba Rao 2009; Zhan and Ng 2006), most research efforts on expansive soil behavior have largely focused on macro scale responses (mainly cyclic volume change and stress-suction relationships) and provided more of descriptive analysis than physical interpretation. Microscopic properties, such as microstructure, have been incorporated in the double-structure model for expansive soil (Alonso et al. 1999, 2005), however, little attention has been paid to the interparticle physicochemical interactions. Wang and Siu (2006a, b) studied the effects of the microstructure and interparticle forces on the mechanical properties of two pure kaolinite samples prepared at different pH values; however, the mechanical responses were related to saturated samples only. Moreover, kaolinite is more easily controlled microscopically than natural expansive soil, which is usually composed of a mix of clay minerals. The physical modeling of the compression and soil–water characteristics of clay samples based on the microstructure and interparticle forces can be referred to in Anandarajah (2000), Yao and Anandarajah (2003), Amarasinghe and Anandarajah (2011), and Anandarajah and Amarasinghe (2012), with the extension of discrete element method and molecular dynamics. This type of modeling is limited to pure clay samples, rather than natural ones with multiple components, and has not yet incorporated the analysis of shear strength.

Here, the physicochemical characteristics and microstructural information are considered microscopic properties because they are associated with the interparticle/surface forces. This research is aimed at improving the understanding of the roles of the microscopic properties in controlling the macroscale behavior, and also providing an experimental database for potential physical simulation of mechanics for natural fine-grained soils. Experimental efforts and comprehensive analysis were undertaken to understand the relationship between the microscopic properties, including physicochemical and microstructural characteristics, and the macro-scale response in terms of the shear strength behavior, of two naturally sampled expansive soils under saturated and unsaturated conditions. Evaluating how microscopic properties affect macro-scale features can be extended for use in the physical modeling of expansive soil behavior.

Microscopic properties of the samples

Geotechnical and physicochemical properties

Investigations were conducted on two soils: one with slight swell potential, named Carnisaw, and one with high swell potential, named Eagle Ford. The former was collected from Le Flore, Oklahoma and the latter was retrieved in Irving, Texas. Carnisaw soil is red brown residual silt with high plasticity, weathered from shale of Pennsylvania age. Eagle Ford soil is yellowish/tan highly plastic clay weathered from fossiliferous clayey shale with sandy shale lenses. The field samples were processed through a No. 10 US sieve prior to laboratory experiments in order to remove occasional coarse sands or gravels. Table 1 lists their geotechnical and physicochemical properties. Common geotechnical tests were performed following ASTM standards (ASTM 2011). The specific surface area (SSA, total) was obtained following the EGME (Ethylene Glycol Monoethyl Ether) surface area determination method (Cerato and Lutenegger 2002). The cation exchange capacity (CEC) data were measured from the 1 N ammonium acetate (CH_3COONH_4) extraction method (Rhoades 1982).

Analysis on point of zero charge

The investigation on the interparticle physicochemical forces involved the point of zero charge (PZC) analysis. Several types of points of zero charge exist. They are derived from different molecular models of surface charge, each corresponding to a specific physical meaning through a particular lab test (Sposito 1998). The point of zero net charge (PZNC) is defined as the pH value at which the intrinsic surface charge, σ_{in}, is zero. The PZNC was suggested as the PZC that is most experimentally accessible and conceptually versatile (Zelazny et al. 1996). Therefore the PZNC is referred to as PZC in this article. An expression of σ_{in} at point of zero net charge gives

$$\sigma_{in} \equiv \sigma_o + \sigma_H = 0 \quad (1)$$

where σ_{in} represents the surface charge density of the adsorbent structure (of a clay particle); σ_o is the net

Table 1 Geotechnical and physicochemical features of Carnisaw and Eagle Ford

Soil property	Carnisaw	Eagle Ford
% Passing No. 200 sieve	84	100
Clay size fraction, CF (% <2 μm)	51	66
Specific gravity, G_s	2.8	2.7
Liquid limit, LL (%)	59	92
Plastic limit, PL (%)	32	35
Plasticity index, PI (%)	27	57
Optimum moisture content, w_{opt} (%)[a]	26.2	27.1
Maximum dry unit weight, γ_{dmax} (kN/m^3)[a]	15.9	14.2
Percent of free swell, s (%)	2.3	12.7
Swell pressure, p_s (kPa)	75	263
pH value (−)	4.4	7.7
Specific surface area, SSA (m^2/g)	107.5	213.5
Cation exchange capacity, CEC (meq/100 g)	27.3	49.6
USCS classification	MH	CH
Vermiculite/montmorillonite (%)[b]	12	28
Illite (%)[b]	25	27
Kaolinite (%)[b]	14	11

USCS Unified Soil Classification System

[a] Standard proctor compaction

[b] Percentages of the entire sample, source: Lin and Cerato (2013a)

permanent surface charge density or structural charge density owing to isomorphous substitution being independent of pH or ionic strength; σ_H is the net proton surface charge density originating from complex protons on hydroxyl groups and varies with pH and ionic strength (Sposito 1992, 1998). When the pH value of the electrolyte surrounding a clay particle falls below the PZC of the related clay mineralogy, the edge of the particle tends to hold positive charge due to migration of the surrounding protons to oxygen ions in the hydroxyls at the aluminum edge sites of the octahedral sheet. On the other hand, a pH above PZC produces negative charges on the edge sites, as the relatively high pH provokes breaking of hydrogen bonds in hydroxyl groups and exposes the negatively charged oxygen ions.

The net total particle surface charge density, σ_p, is given as

$$\sigma_p \equiv \sigma_{in} + \sigma_s = -\sigma_d \quad (2)$$

where σ_s is the stern layer surface charge density, which is a combination of inner-sphere and outer-sphere complex charge densities; σ_d is the surface charge density of the diffused ion swarms or diffuse double layer (DDL). It is worth noting that even though DDL encompasses both the charged surface and diffuse layer, the term DDL is frequently used in lieu of the latter. Obviously, σ_p is balanced by σ_d in order to maintain electrical neutrality. By combining the electric effect of the stern layer with that of the DDL, two simplified conceptual models describing the clay particle associations at different pH conditions relative to the PZC are constructed and illustrated in Fig. 1. It must be noted that the conceptual models in Fig. 1 are relevant for a pure clay sample, which has only one type of clay mineral. In the first model the interparticle interaction is dominated by Coulombic electrostatic force while in the second, the forces are principally DDL repulsion and, to a lesser extent, van der Waals force. The PZC of the clay minerals composing both samples are listed in Table 2.

Unlike pure kaolinite whose pH vs. PZC relationship functions as the determining factor in fabric formation (Wang and Siu 2006a, b), a heterogeneous sample is composed of mixed clay and non-clay minerals that possess various PZCs. Therefore, the surface charge distribution of clay particles is dependent on their individual PZC relative to the pH of the entire sample. Moreover,

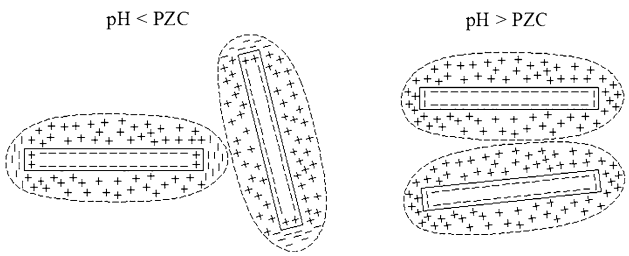

Fig. 1 Interaction of clay particles at different pH conditions

Table 2 Point of zero charges of clay minerals in Carnisaw and Eagle Ford

Mineral	Montmorillonite	Vermiculite	Kaolinite	Illite
PZC	2.5–2.8	8.6–9.3	4.8–7.2	4.6–6.4
Reference	Zelazny et al. (1996); Taubaso et al. (2004); Abollino et al. (2008)	Fox and Malati (1993); Abollino et al. (2008)	Zelazny et al. (1996); Katari and Tauxe (2000); Taubaso et al. (2004)	Katari and Tauxe (2000); Taubaso et al. (2004)

Coulombic interaction can occur between not only clay particles of the same mineralogy but also in between those with differing mineralogy. In Carnisaw (pH = 4.4, Table 1), the constituting clay minerals such as vermiculite, kaolinite and illite tend to get protonated at their particle edges and develop an edge-face flocculated structure as illustrated in the first model of Fig. 1, since all of these three minerals have their PZCs greater than 4.4 (Table 2). On the other hand, the PZCs of the clay minerals in Eagle Ford (corresponding to montmorillonite, kaolinite and illite as given in Table 2) are all smaller than the pH of the soil (pH = 7.7, Table 1), giving rise to the formation of laminar fabric with more substantial face-face particle association, due to the negatively charged edges of the clay particles in such case (illustrated by the second model of Fig. 1). Further evidence in support of the arguments above is achieved from the direct microstructural observations as presented below.

Microstructural implications

It is of vital importance that the intact structures of the soil samples are revealed to provide information for the microstructural implications in the following shear behavior analysis. In this regard, the carefully fractured samples were observed on a field-emission gun environmental scanning electron microscope (FE-ESEM), of which the undesired sample disturbance was minimized. The representative micrographs are shown in Figs. 2, 3, for the initially compacted state, and the consolidated after saturated state, respectively.

In Figs. 2, 3, Carnisaw shows a flocculated structure dominated by the edge-edge and edge-face particle associations. The more plastic Eagle Ford demonstrates a laminar structure with dispersive, larger, thinner clay platelets or aggregates mostly associated in a face-face contact style. Consolidation of both soils following saturation brought about little structural changes attributed to densification. Although not shown here, an increase of consolidation pressure to 400 kPa caused the Carnisaw structure to become more laminar, with intensified the parallel alignment of clay platelets. These findings are consistent with the analytical results of the PZC tests. Also by comparing Figs. 2, 3, a development of DDL, implied by the thickening of clay sheets, visually transforming into a gel-like consistency (Fig. 3), is obvious for the cases of both soils. In addition, although it is desirable to analyze microstructural evolution of the samples along various capillary paths, technical limitations related to the ESEM technique restricted this kind of effort (Lin and Cerato 2014).

Triaxial tests on saturated and unsaturated specimens

Preparation of test specimens

There were 27 specimens prepared for either Carnisaw or Eagle Ford, covering three target suctions, s, close to 2, 5 and 10 MPa, three confining stresses, p_c, of 0.1, 0.2 and 0.4 MPa, and three capillary paths, primary drying (PD), primary wetting (PW) and secondary drying (SD). A suction range of 0–10 MPa was selected to account for most moisture fluctuations expansive soil is exposed to when subjected to alternating flood and drought conditions in the field. The confining pressure as high as 0.4 MPa (400 kPa) encompasses most in-field stress scenarios (equivalent to a 20 m deep overburden pressure if a wet density of 2 Mg/m^3 is assumed). Notice in particular that the suction-control methods (e.g., axis-translation, osmotic and vapor equilibrium techniques) were not considered because of the number of tests designed in this study and the time required to complete a single test.

Initially, the specimens were prepared at their optimum states (w_{opt} and γ_{dmax}, Table 1). After being completely saturated, the specimens were air-dried, rewetted and dried again following a procedure used for the determination of hysteretic soil water characteristic curves (HSWCCs) in Lin and Cerato (2013b), encompassing three drying/wetting paths (PD, PW and SD). Parts of the HSWCCs at suctions greater than 1 MPa are illustrated in Fig. 4. The cylindrical specimens immediately after compaction had a diameter of 35.6 mm (1.4 inch) and a length of 71.1 mm (2.8 inch). Neither filter paper nor geotextile was applied to assist drainage of the specimens because in such plastic samples, the filter paper will get stuck to, and become part of, a specimen, while the soil matrix will penetrate the openings of the geotextile when a specimen is saturated. When the volumetric water content reached the target

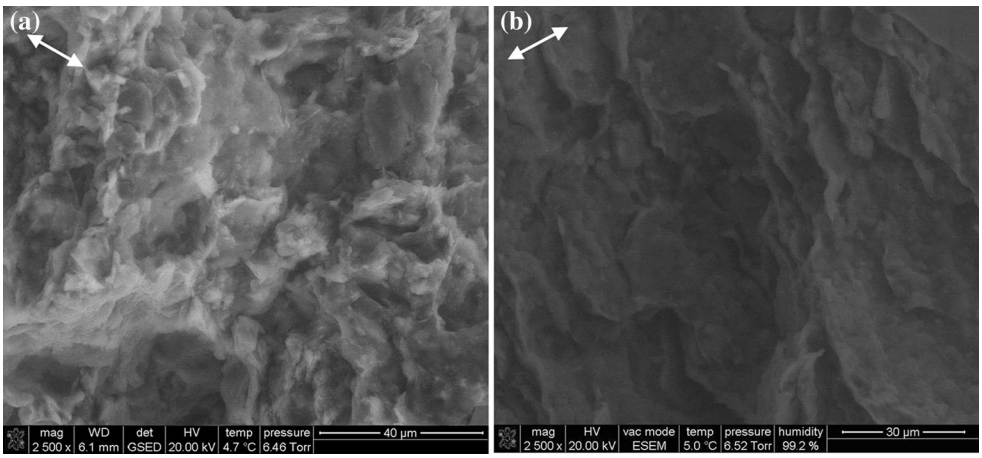

Fig. 2 ESEM micrographs of compacted samples **a** Carnisaw **b** Eagle Ford. *Arrows* denote the directions of compaction (volume-compacted to the optimum state)

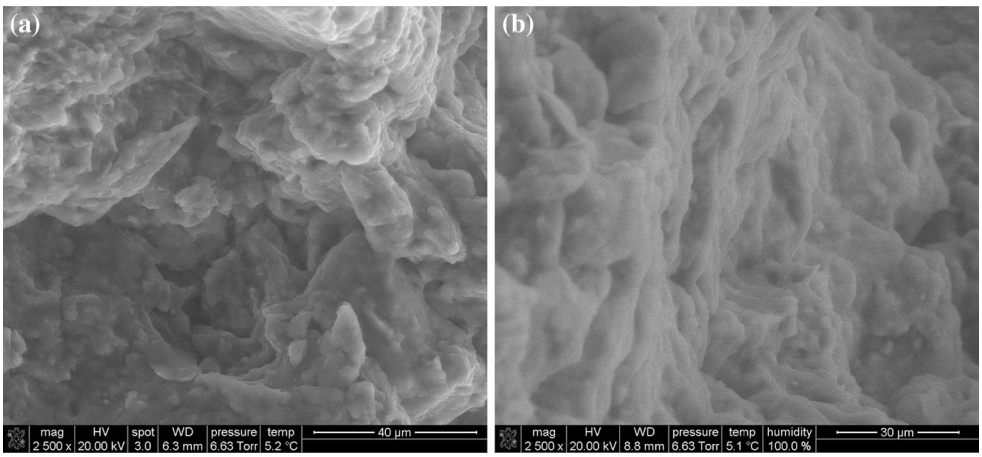

Fig. 3 ESEM micrographs of saturated **a** Carnisaw and **b** Eagle Ford after consolidation at 100 kPa

suction, the specimen was sealed and stored in a 100 % humidity room for moisture equalization that lasted 2–4 months. In reality, the preparation of the specimens always resulted in suction magnitudes that deviated slightly from the volume-mass calculation and the HSWCCs. In addition, it was found from a separate set of specimens (exclusively for evaluation on moisture distribution) that suction distribution throughout the specimen (on every one-fifth of the specimen height) was not completely homogenous, regardless of capillary history. In general, for specimens of low suction (<6 MPa) the suction varied less than 0.2 MPa along the specimen height whereas for specimens of high suction (>10 MPa) the variation was within 0.6 MPa, corresponding to a change of moisture content within 0.5 %. The difference between the average of the measured suction and the estimated value based on the HSWCCs was less than 0.3 MPa. Such a consistency indicates a good homogeneity of the specimens produced by a uniform preparation procedure. Furthermore, the total suction of an unconfined highly clayey sample (with clay size fraction ≥50 %) can be exclusively determined by its moisture content when relatively dry (e.g., $s > 1$ MPa) and was found to be independent of initial dry density (Romero et al. 1999; Miller et al. 2002; Tang et al. 2002). The suction of each of the 54 specimens in unsaturated triaxial tests was measured by chilled mirror hygrometer directly on every one-fifth height of the specimen after shear and thereby averaged. The averaged value deviated from the estimated value based on the pre-determined HSWCCs within ±1.6 MPa. The average value was taken to represent the actual suction of each triaxial specimen. Figure 4 illustrates the hydraulic states of the 54 unsaturated specimens. The slight deviation of the data points from the predetermined HSWCCs resulted from an averaging of the estimated suction (from the HSWCCs) with the measured suction after constant-mass triaxial tests.

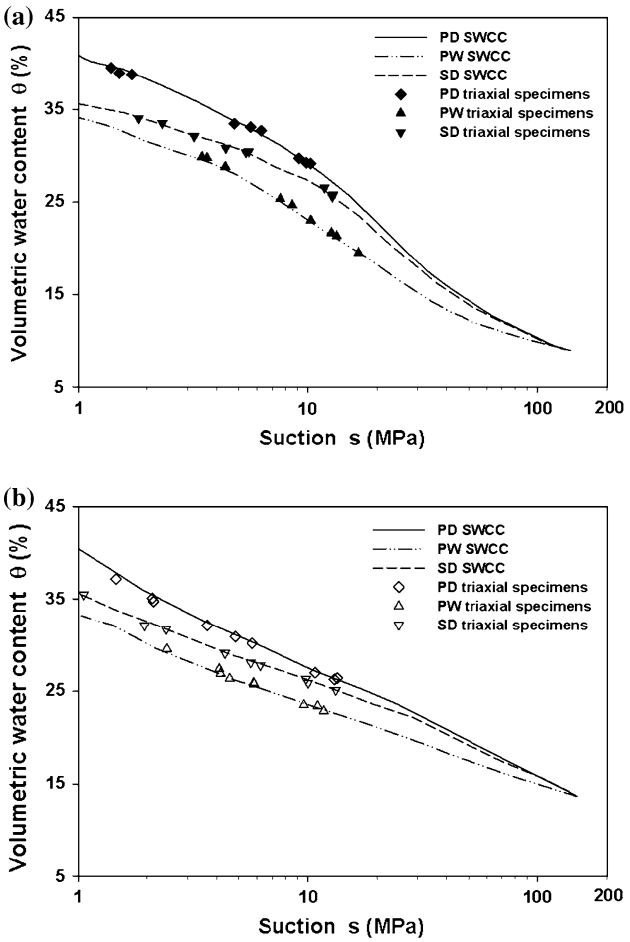

Fig. 4 Hydraulic states of the triaxial specimens relative to the predetermined HSWCCs

Triaxial test program

First, consolidated isotropic undrained compression (CIUC) tests following ASTM-D4767 (2011) were conducted on specimens back-pressure saturated from the initial compacted states (with B value greater than 0.95). A strain rate (1.4×10^{-4} %/s) was used in the CIUC tests, which is much lower than that determined by the criterion of ASTM-D4767 (2011). The specimens were sheared after consolidation under effective stresses of 0.05, 0.1, 0.2 MPa and 0.3 (or 0.4 MPa) until 15 % vertical strain ($\varepsilon = 15$ %) was reached. Secondly, constant-mass confined compression tests were carried out on the unsaturated specimens. These tests comprised of two stages: confining and shearing, through which a drained air phase and an undrained water phase were maintained. A schematic view of the constant-mass test setup is demonstrated in Fig. 5. Two brass porous disks were placed at the top and bottom of each specimen, with both sides covered with a sheet of Teflon (PTFE) filter membrane. The tiny pore dimension of the filter membrane (<5 μm) renders it almost impervious to water while providing access to air, so that the air phase of the specimen was drained throughout the test. The first membrane in direct contact with the specimen worked as a waterproof layer, while the second was used to prohibit atmospheric water vapor from entering the specimen. The porous stone served as a buffer zone to eliminate air pressure buildup on the ends of the specimen during shear. Moreover, a piece of Whatman filter paper (with pore size of 20–25 μm) was inserted between the cap/pedestal and the filter membrane to prevent tearing of the membrane by the notch on the cap/pedestal face (this did occur in some trial tests). The filter paper also improves air flow on the membrane surfaces because it is highly permeable to air. It was further perforated in the center part in contact with the cap/pedestal notch to allow air passage. After each specimen was installed, one more Latex membrane was used to stop leakage caused by potential damage of the first Latex membrane.

The cell pump and the triaxial cell were integrated with an automated load test system which was able to control and record the stress–strain-volume data on an automated stress-path triaxial software platform. The de-airing device was installed at a level slightly higher than the top of the triaxial cell to ensure slow water flow to fill the cell chamber. The planned confining pressure was immediately implemented by the cell pump once the chamber was full of water (Fig. 5). An evaluation of volumetric strain during shear is important when prediction of movements such as settlement is required. However, the volume change monitored through the cell pump is not able to accurately represent the amount of specimen consolidation because the acrylic cell, flow tubes and Plexiglas pedestals also deform and creep under a confining stress. This phenomenon leads to the volume change hysteresis that renders calibration difficult (Lawrence 2004; Houston et al. 2008) and must be solved by adopting an advanced double wall cell plus a volume monitoring system, which was not available for this study.

The confining process was terminated followed by the initiation of shearing as soon as the volume changed slower than 0.01 cm^3/h, which was usually achieved after 1–3 h. At this moment, it was assumed that both the cell deformation and creep of the specimen had stabilized. The shear-induced volume change (with a constant cell pressure) recorded by the cell pump, was therefore estimated as the specimen volume evolution. In this sense, the shear-induced volume evolution was not explicitly presented, but instead implicitly used, to interpret the stress–strain behavior. After the application of confining stresses, the specimens were sheared at a constant rate of 1.4×10^{-4} %/s until 15 % vertical strain ($\varepsilon = 15$ %). The selection of such a strain rate was discussed and evaluated thoroughly in Lin (2012). All the tests took place in room

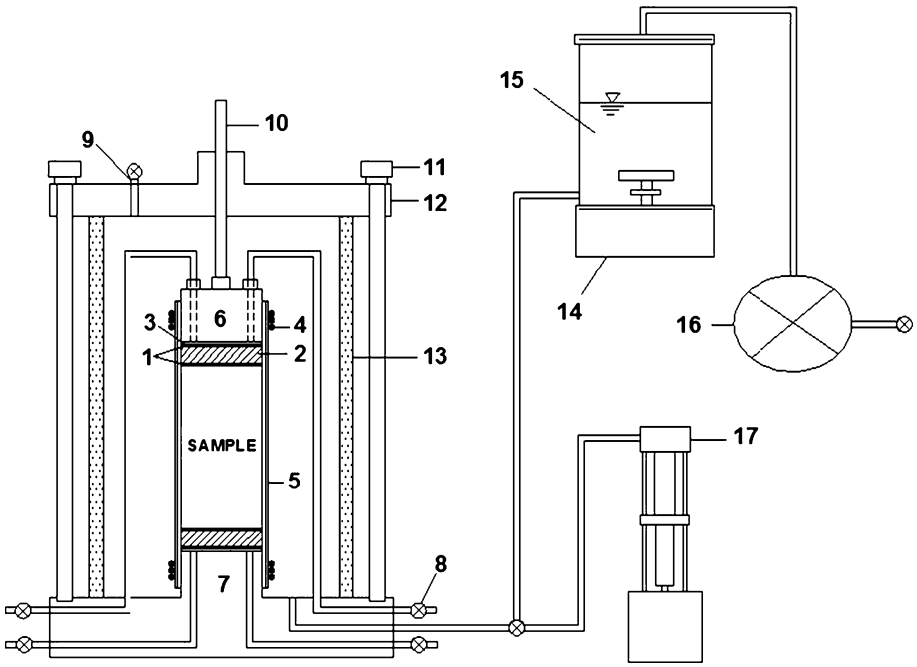

Fig. 5 Schematic view of the constant-mass test setup. *1* Teflon filter membrane, *2* brass porous disk, *3* filter paper, *4* "O" ring, *5* Latex membrane, *6* cap, *7* pedestal, *8* valve, *9* vent port, *10* piston, *11* fastening rod, *12* top frame, *13* acrylic cell, *14* de-air device, *15* water, *16* vacuum pump, *17* cell pump

temperature of 25 ± 0.5 °C. The overall triaxial test program took more than 2 years to finish.

Results and discussion

Stress paths of the saturated specimens

The effective stress paths of saturated Carnisaw and Eagle Ford specimens are plotted jointly in Fig. 6a. The critical state lines record the slope magnitudes of 1.45 and 0.88, the critical-state friction angles (φ_c') of 35.7° and 22.6°, for Carnisaw and Eagle Ford, respectively. In general, Carnisaw exhibits markedly higher shear strength than that of Eagle Ford. At the same time, the specimens of both soils demonstrate responses of contracting initially and then passing through a phase transformation state.

The low pH of Carnisaw (pH = 4.4, Table 1) tends to promote a positive charge at the edge site of the clay particle, owing to its protonation in the acidic environment (Wang and Sui 2006a). This results in an intense edge-face particle association (Figs. 2a, 3a) caused by Coulombic electrostatic forces. On the other hand, the slightly basic acidity of Eagle Ford (pH = 7.7, Table 1) favors the development of negative charges at the edge site and hence a more dispersive fabric as shown by laminar face-face particle association (Figs. 2b, 3b) controlled by both van der Waals attraction and DDL repulsion. However, both soils exhibit dilative responses regardless of their distinct structures. This may be attributed to the closely packed fabric and the strong DDL repulsion during shearing. It is useful to compare the results of this study to those of Wang and Siu (Wang and Sui 2006b) on two kaolinite samples with similar pH and structure (Fig. 6b). It should be noted that both Carnisaw and Eagle Ford are highly plastic expansive soils (PI = 27 and 57, CF = 51 and 66 %; Table 1) with more than 95 % of their particles passing the No. 40 US sieve. No clods greater than a diameter of 1 mm were visualized on the initially compacted specimens (further confirmed by the ESEM observations at a low magnification ratio), implying the relative homogeneity of soil structure of the specimens at their compacted states.

In Fig. 6b, the pH 4 kaolinite specimens showed continuous contraction whereas the pH 7.8 specimens illustrated a phase transformation state and greater shear strength at critical state. In contrast, the Carnisaw (pH = 4.4) specimens of this study, exhibited dilative behavior despite its flocculated "card house" structure and low pH (similar to the pH 4 kaolinite sample). This suggests that mineralogy plays a crucial role in governing the stress–strain behavior of expansive soils. The vermiculite content (Table 1) may contribute to the DDL development and repulsion in Carnisaw. Moreover, the low salt concentration of Carnisaw further enhanced the development of DDL thickness (Lin and Cerato 2013a), which in turn promoted interparticle repulsion. Such repulsion became significant as the Coulombic attraction deteriorated in response to the gradual destructuring of the edge-face associations when shearing proceeded, rendering Carnisaw dilative, though it has a relatively low SSA compared to that of Eagle Ford (Table 1). In Eagle Ford, DDL and repulsion and van der Waals attraction acted as the

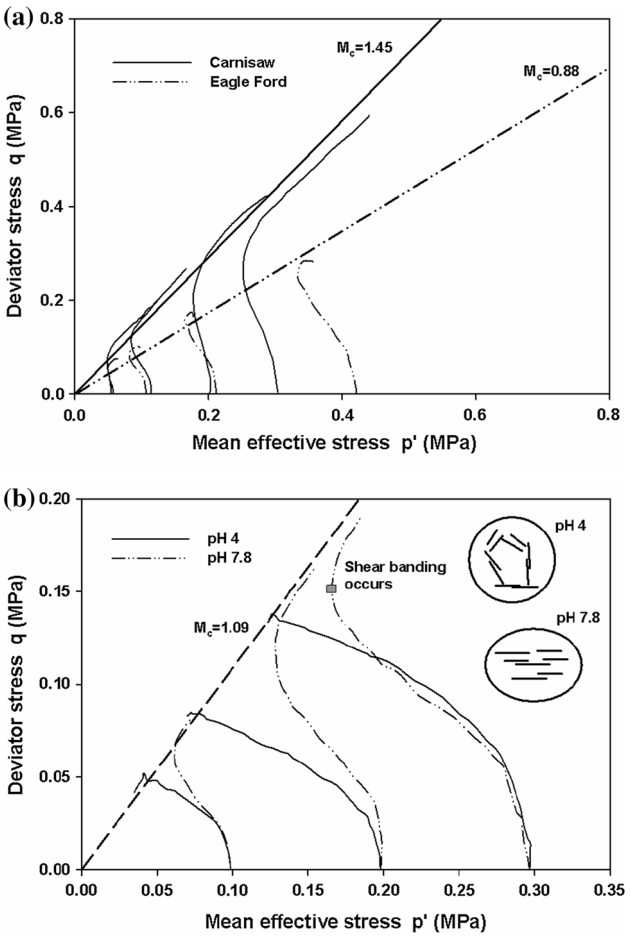

Fig. 6 Effective stress paths of **a** Carnisaw and Eagle Ford specimens study **b** pH 4 and pH 7.8 kaolinite (slightly modified from Wang and Siu (2006b)

prevailing forces on the surfaces of face and edge sites as the particles are brought closer. With shearing, the strength gain from the DDL repulsion on the face-face contact became progressively intensified, which was similar to that observed in Wang and Siu's (2006b) pH 7.8 kaolinite sample.

Effects of mean stress, suction, capillary history and strain level

Since the specimen preparation was carried out based on the HSWCCs, instead of being equilibrated by a suction-controlled method, it is not possible to evaluate the *p*–*q* relationship on a constant-*s* plane, directly from the test points. However, because the suction values were estimated before shearing from the HSWCCs, and measured by the chilled mirror hygrometer afterward and averaged, the *p*–*q* relationship can be revealed from the fitted surface based on the test data. In this aspect, the *p*–*s*–*q* surfaces, instead of individual *p*–*q* and *s*–*q* curves, were numerically fitted (of both peak strength, q_{pk}, and large strain strengths (ε = 14–15 %), q_{ls}) with 9 data points (3 mean stresses times 3 suction magnitudes) forming the basis for each regressed surface. The surfaces were constructed in a conservative way so as to best represent the test data. These fitting efforts were fulfilled by using a quadratic fitting model (Blatz 2000; Blatz et al. 2002). Because constant-*s* planes will be deduced from the fitted surface to represent the actual soil behavior, special care must be focused on defining the boundaries of the surface, as the actual shape of the surface across the entire (*p*, *s*) scopes can be misleading with respect to the shapes of the *p*–*q* relationships. For instance, a specimen of high suction tends to have a large stiffness and is unlikely to fail at a small magnitude of *p* ($p = p_c + q/3$), thus rendering the part of the surface at locations of low *p*/high *s*, physically unsound. In this regard, the boundaries of *p* were set as the minimum and maximum *p* recorded of the test data, and those of *s* were bounded by the minimum and maximum ratios of (*s*/*p*) of the test data. This delimitation resulted in the most conservative surfaces that best represent the actual soil behavior (Lin 2012). On the basis of the fitted surfaces, constant-*p* or constant-*s* planes can be achieved from the regressed surfaces. In order to focus on the effects of the factors like mean stress, suction, capillary history and strain level on the shear strength, the p_{pk}–q_{pk} and p_{ls}–q_{ls} diagrams at suctions of 2 MPa, 5 MPa and 10 MPa, taken from the fitted surfaces, are presented in Figs. 7, 8. The development of peak strength (q_{pk}) and large strain (post peak) strength (q_{ls}) that disclose the shear strength of expansive soil in the field before and after yielding is important to observe. q_{pk} best characterizes the "brittleness" of the test specimens, while q_{ls} is taken to be similar to the "critical state" strength (Blatz et al. 2002), although no measurements have been taken to confirm that state.

The results of CIUC tests are also presented for comparison purposes and these points are taken directly from the actual test results (because suction is zero and no fitting is needed). It must be noted that the *p*–*q* curves from the CIUC tests are test data and representative of effective stress relationships, whereas the curves from the constant-mass tests are fitted, illuminating total stress relationships.

From close inspection of the p_{pk}–q_{pk} and p_{ls}–q_{ls} diagrams (Figs. 7, 8), several interesting findings can be drawn:

1. At an identical *p*, *q* increases with an increase of suction, irrespective of strain level and capillary history. This originates from the greater contraction of meniscus at higher suction that generates a stronger surface tension (capillary) force, which tightens the neighboring particles and strengthens the interparticle normal forces.

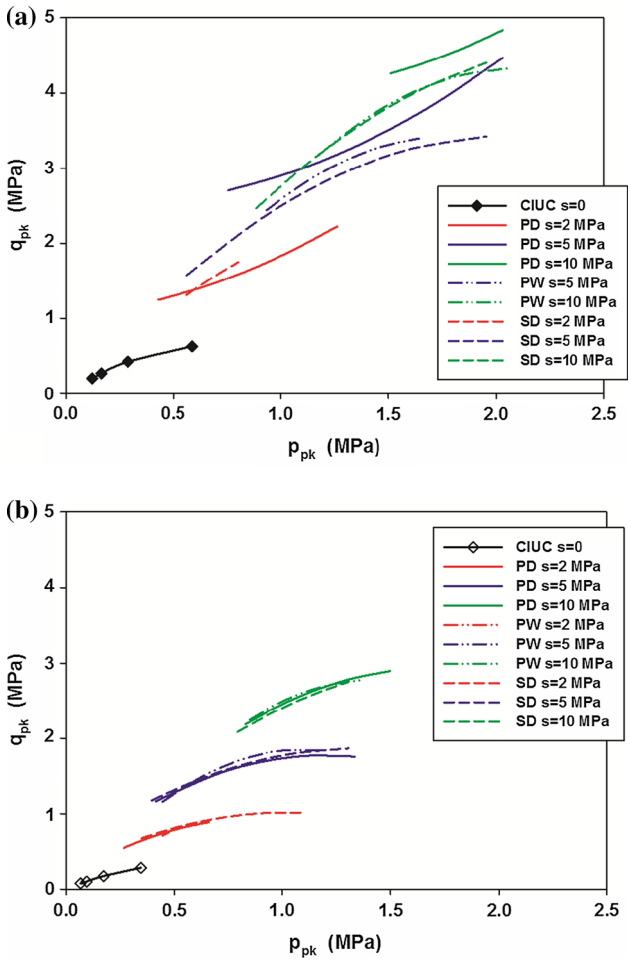

Fig. 7 Peak strength envelopes of **a** Carnisaw and **b** Eagle Ford at varying suctions

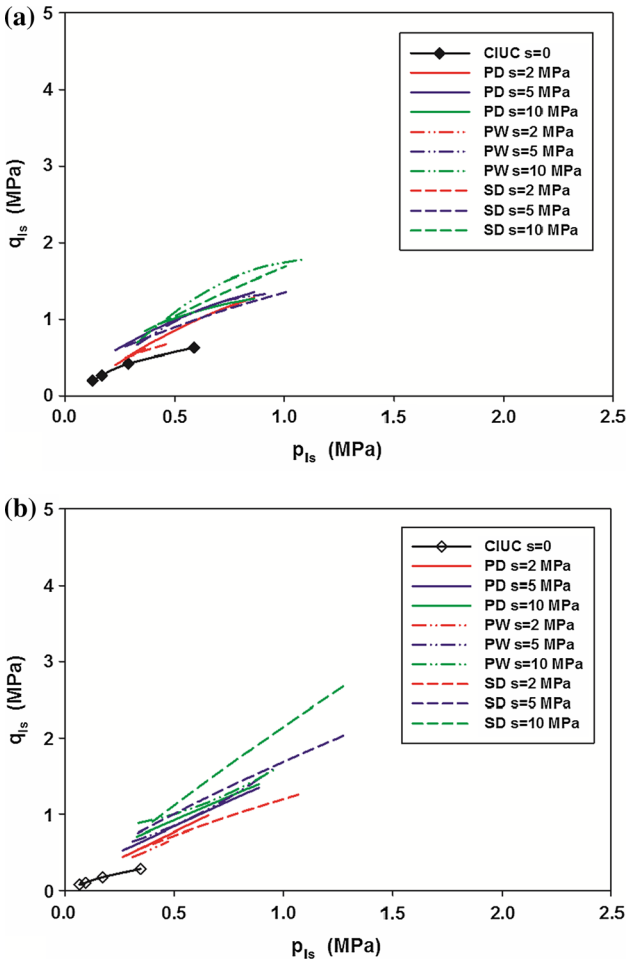

Fig. 8 Large-strain strength envelopes of **a** Carnisaw and **b** Eagle Ford at varying suctions

2. In general, except the p_{pk}–q_{pk} curves representing the PD path of Carnisaw (Fig. 7a), the slopes of the non-linear p–q curves ($\Delta q/\Delta p$) decrease with increasing p (curving downward) but increase with larger s (Figs. 7, 8). This is consistent with Wiebe et al. (1998) and Blatz et al. (2002), though different materials were investigated (50:50 sand-bentonite mixtures in their studies) and no explanations were provided. Tentative efforts are given here to explore the underlying physicochemical mechanisms.

The peak deviator stress, q_{pk}, is controlled by the combined effect of the interlocking of particles/aggregates (Coulombic attraction), DDL repulsion and van der Waals force. At certain large strains, the original specimen is fully destructured where part of the shear resistance contributed by the interlocking effect is gone and then the resistance, q_{ls}, is exclusively controlled by the interparticle repulsion and subsequent slipping carried by the DDL, with van der Waals force relatively unaffected by the structural changes. The contractive resistance attributed to Coulombic attraction as well as soil dilatancy created by the DDL repulsion in response to shearing are solely dependent on the intrinsic physicochemical characteristics of the soil. In the case of the PD p_{pk}–q_{pk} curves of Carnisaw (Fig. 7), the contractive resistance is significant due to a substantial development of the flocculated "card-house" fabric, and its contribution to shear strength increases with p_{pk}; whereas, for the rest of the p_{pk}–q_{pk} curves of both soils, the dilative effect plays the predominant role and weakens with p_{pk} (Fig. 7), since the associated fabric is more parallel packed (the structural development with capillary path will be discussed later). The latter case applies to all the p_{ls}–q_{ls} curves of the large strain case (Fig. 8) because specimen destructuring removes the interlocking effect, though illustrated in a less explicit way due to the insufficient shear strain implemented (the maximum axial strain was taken at 14–15 %). These $\Delta q/\Delta p$ tendencies should be further verified by a detailed exploration using molecular dynamics, which was not achieved at this point. The increasing suction tends to thwart the destructuring of the specimen and

the initiation of the fully-developed dilation, due to the stronger interparticle bounding caused by surface tension. Consequently, the p–q slopes increase with increasing suction. It is worth mentioning that part of the specimen dilation may also be affected by the "roll-over" effect of the clay aggregates similar to the behavior of sand when the specimen is significantly dry, though further research is needed to justify this mechanism.

An increase in either suction, s, or mean stress, p, results in an increase of the deviator stress q, because both s and p contribute to the enhancement of the interparticle bounding and interlocking of aggregates. This phenomenon reveals itself as an increase of the specimen density. The density change, due to the contribution of s, is evaluated on all the specimens immediately after their preparation (Fig. 9). Despite the scattering of data, a distinct trend of slight density increase with increasing s (though it is hard to distinguish the effects of hydraulic hysteresis on the density evolution) can be observed. The impact of confining stress upon density was difficult to evaluate since the volume measurement during confinement was unreliable. Instead, the role of the mean stress, p, can be reasonably analyzed from Figs. 7 and 8 (as previously discussed). An increase of p causes the collapsing of inter-aggregate macropores (e.g., macropores formed by the "card house" fabric) and intensified packing of particles and aggregates, resulting in a greater density.

The fact that p and s are inter-related creates a challenge in separating their influences on the density and shear strength of clayey soils. An increase in the dry density of an unsaturated specimen can be either attributed to pressure loading (Δp) or shrinkage (Δs). On one hand, an increase of p compresses the air phase of a specimen and results in a greater saturation ratio. On the other hand, suction increase enhances the shear resistance of a specimen; i.e., a specimen of a greater s tends to fail at a larger p ($p_f = p_c + q_f/3$). Therefore, any experimental description for the yielding of a highly plastic soil on a constant-p or constant-s plane becomes problematic, while in literature, p and s are commonly used as independent stress variables in the elastoplastic modeling of highly plastic soils (Alonso et al. 1990; Wheeler and Sivakumar 1995; Delage and Graham 1995; Cui and Delage 1996; Alonso et al. 1999). Other researchers (Tang and Graham 2002; Blatz and Graham 2003) coupled the effects of p and s on the yielding behavior. This type of coupling rendered the use of individual p and s coordinates in constructing the yield surface in a p–s–q space controversial (Blatz and Graham 2003). Future research is needed to evaluate the individual role of p and s in the structure evolution of an unsaturated fine-grained sample during confinement and shearing.

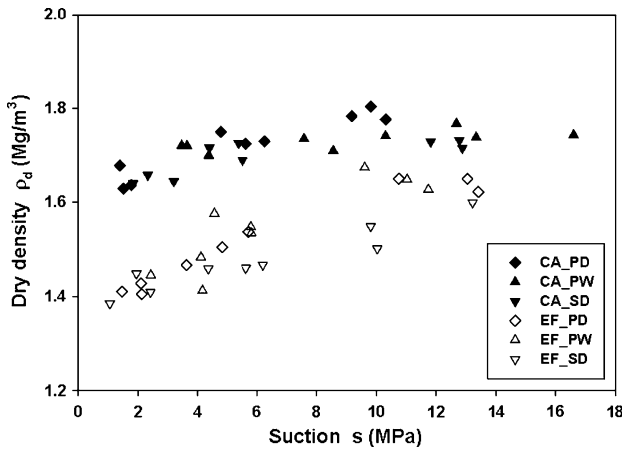

Fig. 9 Impact of suction on the dry density

3. Capillary history has a dramatic impact on the p_{pk}–q_{pk} envelopes of Carnisaw (Fig. 7a) while playing a much less significant role on its p_{ls}–q_{ls} curves (Fig. 8a). In the case of Eagle Ford, a distinct feature is highlighted in that the effect of suction history becomes negligible with respect to the p_{pk}–q_{pk} relationships, as the p_{pk}–q_{pk} curves of the specimens with same suction surprisingly overlap each other (Fig. 7b). However, when examining the p_{ls}–q_{ls} curves shown in Fig. 8b, a phenomenon showing the strengthening of q of the SD path relative to the other two paths (PD and PW) is identified. The reasons are explained in the following paragraphs.

After several shrink-swell cycles, the macropores collapse generating irreversible plastic strains. These plastic strains gradually decrease, and the microstructure of expansive soils approaches an equilibrium state (Alonso et al. 1995, 1999; Romero et al. 1999; Tripathy et al. 2002, Tripathy and Subba Rao 2009; Nowamooz and Masrouri 2008; Romero and Simms 2008). This will ultimately result in a prevailing structure featured by parallel particle orientation (i.e., face-face particle association) filled mostly by micropores. In other words, the dual-structure of the original sample gradually transforms to an exclusive structure characterized by parallel association of platy clay particles, as a result of the destruction and reorientation of the structural elements of an aggregate or cluster. Understanding this particular nature of expansive soils, it is reasonable to see the distinct p_{pk}–q_{pk} curve of the PD path of Carnisaw by taking into account the flocculated structure dominated with edge-face contacts. The p_{pk}–q_{pk} curves of Carnisaw switch from a shape curving upward to curving downward from the PD to PW path, and the curves representing the SD path remain curved downward (Fig. 7a). Additionally, the corresponding q_{pk} decreases at a given p_{pk}. This is best illustrated in Fig. 7a from comparing the curves of PD, PW and SD at s equal to 5 MPa. The strength decrease comes from the gradual loss of Coulombic attractive forces at the edge-face contacts. In contrast, the

laminar Eagle Ford tends to develop constant interparticle forces and demonstrates the independency in the shear strength of the capillary paths (Fig. 7b).

The coupled effects of the initial structure and the interparticle forces are also implied by Fig. 8. At large shear strains, the plastic zone of the specimen is completely destructured and thus independent of the original structure. As discussed earlier, the shear strength at this point is controlled by the the DDL repulsion-induced dilation. An apparent increase in $\Delta q_{ls}/\Delta p_{ls}$ is noticed on the SD path in Fig. 8b. This specific behavior may be attributed to the effect of aging that imparts resistance to compression (Subba Rao and Tripathy 2003).

Conclusions and summary

This study evaluates the roles of microscopic properties of two natural expansive soils in controlling their macro-scale behavior, in terms of shear strength along different capillary paths. The effects of original structure, mean stress, suction, capillary history and strain level on the shear strength are factored in the microscopic characteristics, integrating both physicochemical and microstructural information. Major conclusions can be reached as follows.

The PZC was used to analyze the interparticle electrostatic bonding or repulsion through the medium known as DDL. For natural samples composed of mixed minerals, the PZC of each composing clay mineral must be evaluated for its relativity to the pH of the entire sample, in order to identify the charge distribution around each kind of clay particle. As such, Carnisaw is prone to form edge-face particle association whereas face-face fabric formation is typical in Eagle Ford. These orientations are created from the positively charged edges of clay particles in Carnisaw and the negatively charged edges in Eagle Ford, while isomorphous substitution of the silicate framework always leaves behind negative charges on the particle faces of both soils. The postulated microstructures of both soils, based on the physicochemical analysis, were confirmed through ESEM observations on the samples under different hydraulic and mechanical states.

For the saturated specimens, Carnisaw has a higher critical-state friction angle than Eagle Ford. The specimens of both soils demonstrated exactly the same style of response of contracting initially, passing through a phase transformation state, and then dilating (increasing in tendency to dilate) with a constant stress ratio. The interparticle interactions of the Carnisaw specimens were initially dominated by strong Coulombic electrostatic attraction but then transformed to intense DDL repulsion due to shear-induced destructuring of the fabric. The Eagle Ford specimens, on the other hand, were first governed by DDL repulsion and van der Waals attraction and then strengthened in the repulsion part that caused dilation in shearing.

The effects of mean stress, suction, capillary history and strain level on the shear strength were assessed through the studies of the p_{pk}–q_{pk} and p_{ls}–q_{ls} curves with varying suction. The deviator stress, q, increases with increasing suction, regardless of strain level and capillary history, because of the enhanced surface tension force. In general, the slopes of the p–q curves reduce as a function of p and increase with s. The p_{pk}–q_{pk} slope increases with p for the case of the primary drying curves of Carnisaw as a result of its significant development of the Coulombic attraction force at this stage. For both p_{pk}–q_{pk} and p_{ls}–q_{ls} curves, the strengthened s introduces an enhanced surface tension force and hence restrains the progress of fabric destructuring and specimen dilation in response to shearing. Capillary history shows its maximum impact on the p_{pk}–q_{pk} curves of Carnisaw arising from the remarkable structural evolution along the capillary paths. The more homogeneous structure of Eagle Ford renders itself less susceptible to the capillary history change in respect to its p_{pk}–q_{pk} curves. The p_{ls}–q_{ls} curves, however, demonstrate little dependency of capillary history, regardless of soil type because at this point the specimens have the fabric completed destructed and the DDL equilibrated.

Several challenges emerge when investigating the roles played by microscopic properties in governing the macro-scale mechanical response. For instance, on a micro-scale a density increase can be thought of as an intensified packing of particles and thereof a stronger interparticle normal force. In consequence, the shear strength of a specimen increases. However, the mechanisms responsible for the density increase can be either contraction of meniscus (rising suction) or mechanical compression of fabric (increasing mean stress). Therefore, isolating the effects of these mechanisms is a challenge to be solved. Also, a more comprehensive study on the shear strength of the unsaturated expansive soil specimens should include a broader range of confining stress as well as accurate suction control of the specimen, which requires sophisticated equipment compliance and substantial time spent in moisture equilibration. Last but not least, physical modeling of the macro-scale behavior of natural expansive soil samples has to account for interparticle interaction between clay and non-clay particles and also include accurate quantification of various microscopic forces.

Acknowledgments We would like to express our gratitude to the U.S. National Science Foundation (Grant No. 0746980), and the National Natural Science Foundation of China (Grants No. 51404281, 51325402, 51490650, 51174217 and 51234006) for their financial supports. Our research was also supported by the Foundation of State

Key Laboratory of Petroleum Resources and Prospecting (Grant No. PRP/indep-4-1309) and the Science Foundation of China University of Petroleum, Beijing (Grant No. 2462013YJRC037).

References

Abollino O, Giacomino A, Malandrino M, Mentasti E (2008) Interaction of metal ions with montmorillonite and vermiculite. App. Clay Sci 38:227–236

Alonso EE, Gens A, Josa A (1990) A constitutive model for partially saturated soils. Géotechnique 40(3):405–430

Alonso EE, Lloret A, Gens A, Yang DQ (1995) Experimental behavior of highly expansive double-structure clay. Unsaturated Soils 1995:11–16

Alonso EE, Vaunat J, Gens A (1999) Modeling the mechanical behavior of expansive clays. Eng Geol 54:173–183

Alonso EE, Romero E, Hoffmann C, García-Escudero E (2005) Expansive bentonite-sand mixtures in cyclic controlled-suction drying and wetting. Eng Geol 81:213–226

Al-Rawas A (1999) The factors controlling the expansive nature of the soils and rocks of northern Oman. Eng Geol 53:327–350

Amarasinghe PM, Anandarajah A (2011) Influence of fabric variables on clay-water-air capillary meniscus. Can Geotech J 48:987–995

Anandarajah A (2000) Numerical simulation of one-dimensional behavior of a kaolinite. Géotechnique 50(5):509–519

Anandarajah A, Amarasinghe PM (2012) Microstructural investigation of soil suction and hysteresis of fine-grained soils. J Geotech Geoenviron Eng 138(1):38–46

ASTM (2011) 2011 Annual Book of ASTM Standards. Volume 04.08 Soil and Rock (I): D420–D5876 and Vol. 4.09 Soil and Rock (II): D5877—latest. West Conshohocken, Pennsylvania

Blatz JA (2000) Elastic-plastic modeling of unsaturated high plastic clay using results from a new test with controlled suction. Ph.D. dissertation, Dept. Civil. Geol. Eng., University of Manitoba, Winnipeg, MB

Blatz JA, Graham J (2003) Elastic-plastic modeling of unsaturated soil using results from a new triaxial test with controlled suction. Géotechnique 53(1):113–122

Blatz JA, Graham J, Chandler NA (2002) Influence of suction on the strength and stiffness of compacted sand-bentonite. Can Geotech J 39:1005–1015

Cerato AB, Lutenegger AJ (2002) Determination of surface area of fine-grained soils by the ethylene (EGME) method. Geotech Test J 25(3):315–321

Cui YJ, Delage P (1996) Yielding and plastic behavior of an unsaturated compacted silt. Géotechnique 46(2):291–312

Delage P, Graham J (1995) Understanding the behavior of unsaturated soils requires reliable conceptual model state of the art report. In: Proceedings of 1st Int. Conf. on unsaturated soils, Paris, France, pp 1223–1256

Delage P, Howat M, Cui YJ (1998) The relationship between suction and swelling properties in a heavily compacted unsaturated clay. Eng Geol 50(1–2):31–48

Escario V, Saez J (1986) The strength of partly saturated soils. Géotechnique 36(3):453–456

Fjar E, Holt RM, Raaen AM, Risnes R, Horsrud P (2008) Petroleum related rock mechanics, 2nd edn. Elsevier Science, NewYork, p 514

Fox I, Malati MA (1993) An investigation of phosphate adsorption by clays and its relation to the problems of eutrophication of the river stour Kent. J Chem Tech Biotechnol 57:97–107

Houston SL, Perez-Garcia N, Houston WN (2008) Shear strength and shear-induced volume change behavior of unsaturated soils from a trixial test program. J Geotech Geoenviron Eng 134:1619–1632

Ito M, Azam S (2010) Determination of swelling and shrinkage properties of undisturbed expansive soils. Geotech Geol Eng 28:413–422

Katari K, Tauxe L (2000) Effects of pH and salinity on the intensity of magnetization in redeposited sediments. Earth Planet Sci Lett 181:489–496

Lawrence CA (2004) Development of a closed-loop, hydraulically actuated testing system and methodologies for unsaturated soils. Ph.D. Dissertation, Arizona State University, Arizona, USA, May 2004

Lin B (2012). A comprehensive investigation on microscale properties and macroscopic behavior of natural expansive soils. Ph.D dissertation, University of Oklahoma, p 186

Lin B, Cerato AB (2013a) Electromagnetic properties of natural expansive soils under one-dimensional deformation. Acta Geotech 8(4):381–393

Lin B, Cerato AB (2013b) Hysteretic soil water characteristics and cyclic swell-shrink paths of compacted expansive soils. B Eng Geol Environ 72(1):61–70

Lin B, Cerato AB (2014) Application of SEM and ESEM in microstructural investigation of shale-weathered expansive soils along swelling-shrinkage cycles. Eng Geol 177:66–74

Miller CJ, Yesiller N, Yaldo K, Merayyan S (2002) Impact of soil type and compaction conditions on soil water characteristic. J Geotech Geoenviron Engs 128(9):733–742

Nelson JD, Miller DJ (1992) Expansive soils: problems and practice in foundation and pavement engineering. John Wiley and Sons, New York, p 253

Nowamooz H, Masrouri F (2008) Hydromechanical behavior of an expansive bentonite/silt mixture in cyclic suction-controlled drying and wetting tests. Eng Geol 101:154–164

Punthutaecha K, Puppala AJ, Vanapalli SK, Inyang H (2006) Volume change behaviors of expansive soils stabilized with recycled ashes and fibers. J Material Civil Eng 18(2):295–306

Rhoades JD (1982) Cation exchange capacity. In: Page AL et al (eds) Methods of soil analysis, agronomy 9, 2nd edn. American Society of Agronomy, Madison, pp 159–165

Romero E, Simms PH (2008) Microstructural investigation in unsaturated soils: a review with special attention to contribution of mercury intrusion porosimetry and environmental scanning electron microscopy. Geotech Geol Eng 26:705–727

Romero E, Gens A, Lloret A (1999) Water permeability, water retention and structure of unsaturated compacted Boom clay. Eng Geol 54:117–127

Sposito G (1992) Characterization of particle surface charge. In: Buffle J, van Leeuwen HP (eds) Environmental particles, vol 1. Lewis Publ, Boca Raton, pp 291–314

Sposito G (1998) On points of zero charge. Environ Sci Tech 32(19):2815–2819

Subba Rao KS, Tripathy S (2003) Effect of aging on swelling and swell-shrink behavior of a compacted expansive soil. Geotech Test J 26(1):36–46

Tang GX, Graham J (2002) A possible elastic-plastic framework for unsaturated soils with high-plasticity. Can Geotech J 39:894–907

Tang GX, Graham J, Blatz J, Gray Malcolm, Rajapakse RKND (2002) Suctions, stresses and strengths in unsaturated sand-bentonite. Eng Geol 64:147–156

Taubaso C, Dos Santos Afonso M, Torres Sanchez RM (2004) Modelling soil surface charge density using mineral composition. Geoderma 121(1–2):123–133

Tripathy S, Subba Rao KS (2009) Cyclic swell-shrink behavior of a compacted expansive soil. Geotech Geol Eng 27:89–103

Tripathy S, Subba Rao KSS, Fredlund DG (2002) Water content-void ratio swell-shrink paths of compacted expansive soils. Can Geotech J 39:938–959

Wang YH, Sui WK (2006a) Structure characteristics and mechanical properties of kaolinite soils. I. Surface charge and structural characterization. Can Geotech J 43:587–600

Wang YH, Sui WK (2006b) Structure characteristics and mechanical properties of kaolinite soils. II. Effects of structure on mechanical properties. Can Geotech J 43:601–617

Wheeler SJ, Sivakumar V (1995) An elasto-plastic critical state framework for unsaturated soil. Géotechnique 45(1):35–53

Wiebe B, Graham J, Tang GX, Dixon D (1998) Influence of pressure, saturation, and temperature on the behavior of unsaturated sand-bentonite. Can Geotech J 35:194–205

Yao M, Anandarajah A (2003) Three-dimensional discrete element method of analysis of clays. J Eng Mech 129(6):585–596

Zelazny LW, He L, Vanwormhoudt A (1996) Charge analysis of soils and anion exchange. In Methods of Soil Analysis, Part 3. Chemical Methods—SSSA Book Series no. 5, pp 1231–1253

Zhan TLT, Ng CWW (2006) Shear strength characteristics of an unsaturated expansive clay. Can Geotech J 43:751–763